

LA-7869

C.3

**Mach Stems Formed by Colliding
Cylindrical Detonation Waves**

University of California



LOS ALAMOS SCIENTIFIC LABORATORY

Post Office Box 1663 Los Alamos, New Mexico 87545

This work was supported by the US Department of Energy, Office of Military Application.

This report was prepared as an account of work sponsored by the United States Government. Neither the United States nor the United States Department of Energy, nor any of their employees, nor any of their contractors, subcontractors, or their employees, makes any warranty, express or implied, or assumes any legal liability or responsibility for the accuracy, completeness, or usefulness of any information, apparatus, product, or process disclosed, or represents that its use would not infringe privately owned rights.

LA-7869

UC-34

Issued: September 1979

Mach Stems Formed by Colliding Cylindrical Detonation Waves

Charles L. Mader
Douglas Venable



LOS ALAMOS NATL LAB LIBS
3 9338 00203 0160



MACH STEMS FORMED BY COLLIDING CYLINDRICAL DETONATION WAVES

by

Charles L. Mader and Douglas Venable

ABSTRACT

Radiographic studies of laterally colliding, diverging, cylindrical detonation waves in PBX 9404 are reproduced numerically by use of the two-dimensional Lagrangian hydrodynamic code 2DL with a shock initiation burn model called Forest Fire. The formation and growth of a Mach stem is described.

I. INTRODUCTION

Al'Tshuler et al.¹ have experimentally studied shock waves interacting in aluminum to form both regular and Mach shock reflections, and Mader² has reproduced the interaction using the numerical two-dimensional Lagrangian hydrodynamic code 2DL. The calculated Mach stems in aluminum were not well described by the usual simple three-shock model. The stems are curved significantly and are described better by a multiple-shock process with a slip region than by a three-shock process with a slip plane. The calculated growth angle of the aluminum Mach stem increased with increasing collision angle up to nearly 90° where there is a sharp discontinuity.

Attempts² to study colliding detonation waves from homogeneous explosives such as nitromethane by use of resolved reaction zones were unsuccessful because the orders-of-magnitude change in thickness between the regular reaction zone and the Mach stem reaction zone could not be resolved numerically.

Gardner and Wackerle³ used radiographic and rotating mirror camera techniques to study the interaction of plane detonation waves from Composition B, PBX 9404, Baratol, and nitromethane. They

observed that Mach stems and reflected shocks displayed substantial curvature and anomalous density regions and concluded that their observations could not be reproduced using the usual three-shock models.

Lamborn and Wright,⁴ using streak cameras and ionization probes, determined the growth rate of Mach stems formed between two plane intersecting detonation waves in Composition B at various angles of incidence. The three-shock model predicted growth angles about four times larger than those observed. Lamborn and Wright concluded that the theory must include the effect of the reaction zone, the Taylor wave, and the signal emanating from the place where the waves first intersect. They also concluded that two-dimensional numerical hydrodynamics was required. They performed such a calculation with encouraging results, but the crude mesh they used prevented detailed comparison with the experimental data.

In 1969 Venable made a series of radiographic studies of two laterally colliding, diverging cylindrical detonation waves in PBX 9404 (94/3/3 HMX/nitrocellulose/tris- β -chloroethyl phosphate). The results, described in Sec. II, are similar to those

reported previously, in that the Mach stems are substantially curved and contain anomalous density regions. Numerical simulation of the experiments appeared hopeless as long as the problem of resolving the reaction zone could not be solved or circumvented.

Development of the Forest Fire model⁵ of shock initiation of heterogeneous explosives has provided a technique for realistic numerical simulation of the burning region of the regular detonation wave and the Mach stem.

The Forest Fire model can describe the decomposition caused by hot spots formed by shock interactions with density discontinuities which apparently dominates detonation wave propagation in heterogeneous explosives. Forest Fire has been used to describe the passage of a heterogeneous detonation wave around a corner and along metal surfaces. It also has been used to model the failure of propagation of heterogeneous detonation waves which depends on the interrelated effects of the wave curvature and the shock sensitivity of the explosive. The Forest Fire model is therefore an obvious choice for numerically simulating the important features of the burning regions of interacting detonation waves.

II. EXPERIMENTAL STUDIES

Radiographic observations of the progress of two laterally colliding, diverging cylindrical detonation waves in PBX 9404 ($\rho_0 = 1.843 \text{ g/cm}^3$) have been made using PHERMEX.⁶ Figure 1 shows the experimental arrangement. Line wave generators served to initiate these waves. Figures 2-6 show the radiographs. The space-time histories of the detonation wave and of the interaction region that starts

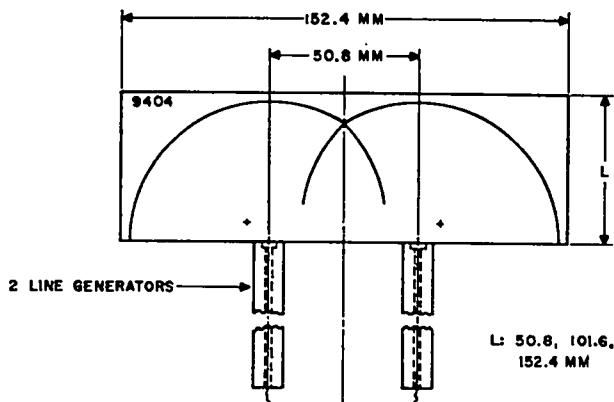


Fig. 1.
The experimental setup.

with regular reflection and subsequently develops into Mach reflection have been measured. This interaction range covers angles of incidence, with respect to the plane of symmetry, from zero to about 85° ; the Mach wave is born at about 50° . Figure 7 shows the data on the radial motion, $r(t)$, of the detonation wave and a similar trajectory, $y(t)$, of the Mach wave. Unless otherwise stated, the excursions are normalized with respect to the value a , which is half the distance between the line generator centers. Real time, t , has been normalized with respect to a characteristic time, defined as $t D/a$, where D is the detonation wave velocity. Figure 7 also shows the computed trajectory of the intersection of the two waves in the regular reflection mode (dashed line), assuming truly cylindrical waves; one radiographic observation point for this region is included.

Both radiography and pins were used to measure the space-time history of the detonation and Mach waves. A linear least-squares fit to the data points on the detonation wave trajectory yielded a wave velocity of $8.745 \pm 0.016 \text{ mm}/\mu\text{s}$, roughly 1% lower than the 8.80 that is normally taken to be the velocity, D , of a plane detonation wave in PBX 9404 of the same density. Note that this difference is also roughly the limit of our present velocity measurement capability, so we can only say that the detonation wave velocity is nearly constant. On the other hand, the Mach wave velocity beginning at its point of origin clearly exceeds $12 \text{ mm}/\mu\text{s}$, considerably more than that of the detonation wave, and then slows, asymptotically approaching the detonation wave velocity. Figure 8 compares these two velocities.

Because the radiographs were made with the beam aligned along the centerline of, but above, the Mach wave, neither of the three-wave-interaction regions was in line, so they are not displayed sharply. Nonetheless, the radiographs show that the reflected wave suffers considerable refraction at late times in the narrow high-density zone behind the detonation wave front.

Radiographs also show that, out to wave radii as great as 150 mm, the high density behind the detonation wave drops off much more rapidly than that behind plane waves.

As already mentioned, the precision of some of the measurements is limited by technique and instrumentation. Another limit is associated with the acylindricity of the waves. The "line wave

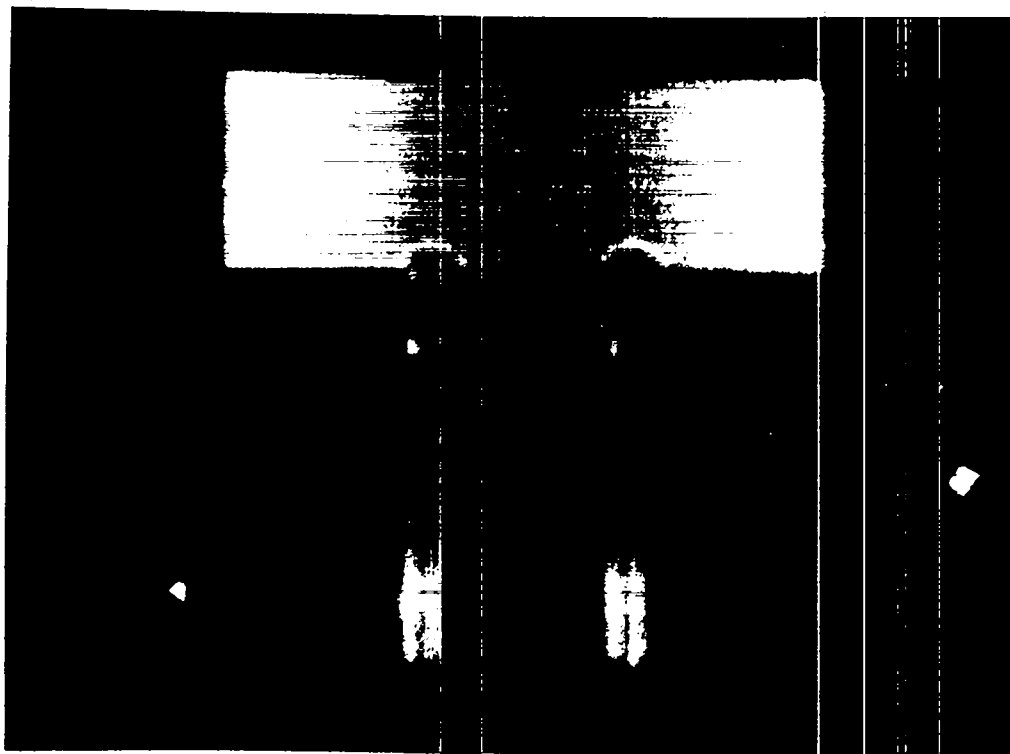


Fig. 2.
Radiograph 1130 at 1.06 μ s after arrival of the line generator shock wave.

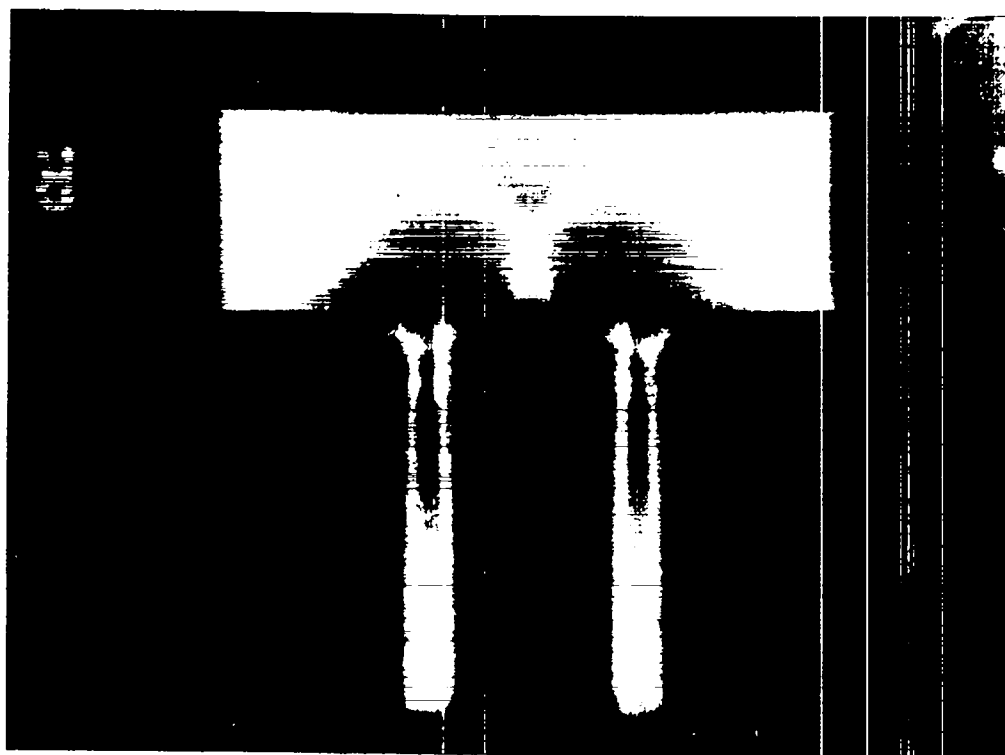


Fig. 3.
Radiograph 1143 at 4.03 μ s after arrival of the line generator shock wave.

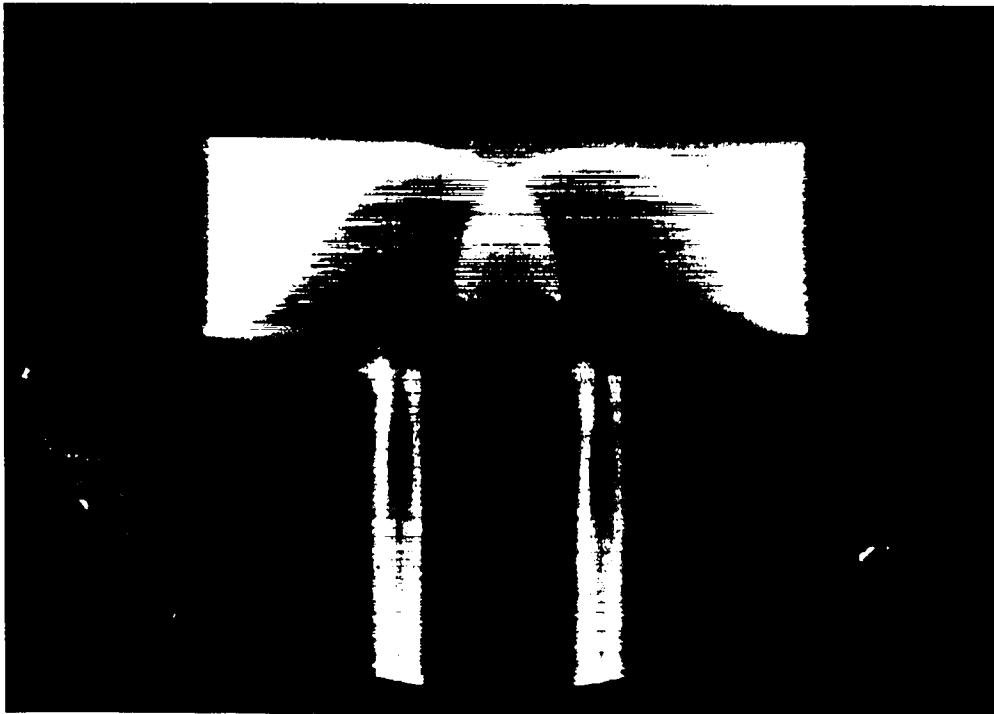


Fig. 4.
Radiograph 1019 at 5.61 μ s after arrival of the line generator shock wave.

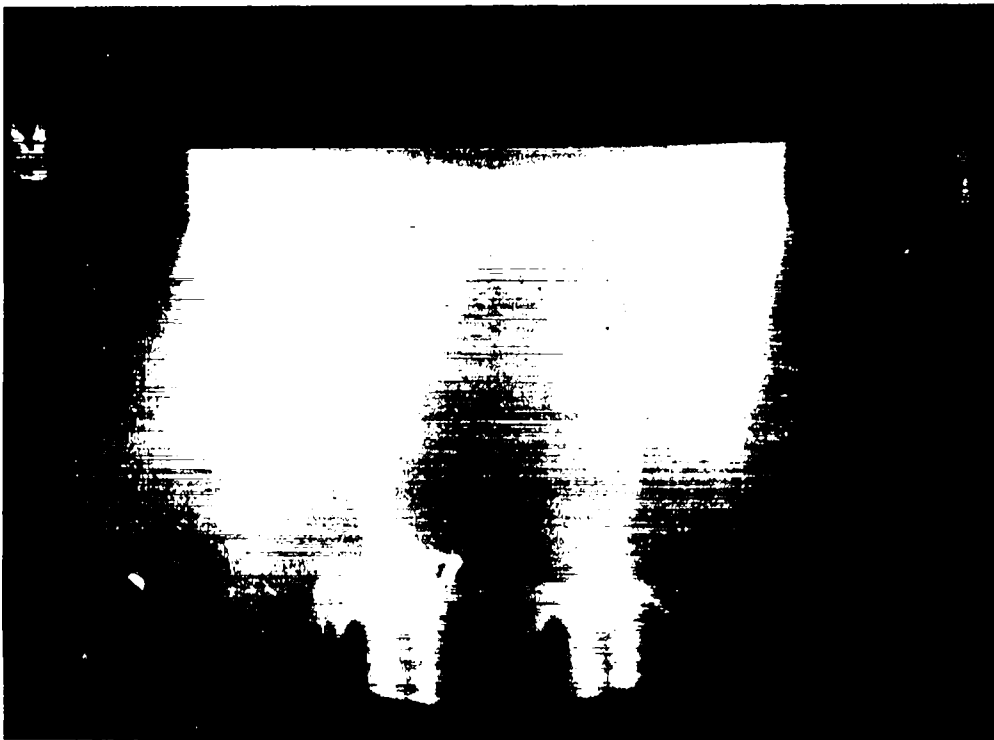


Fig. 5.
Radiograph 1037 at 11.16 μ s after arrival of the line generator shock wave.

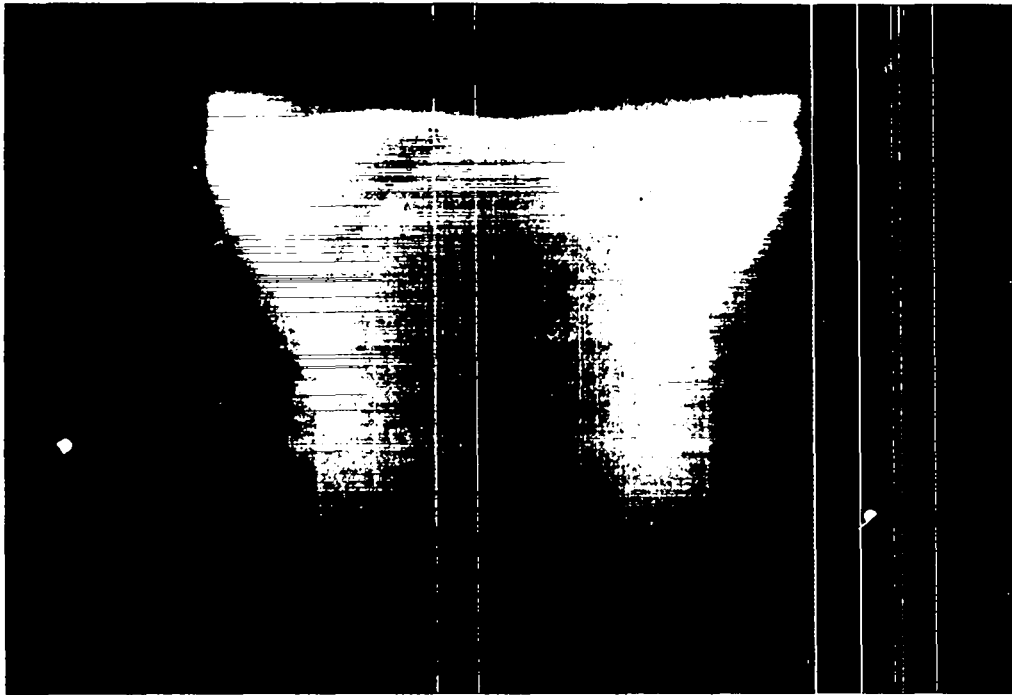


Fig. 6.
Radiograph 1038 at 16.75 μ s after arrival of the line generator shock wave.

generators" are not line generators; they only approximate that function for large-radius waves. The initiating zone in each line generator is about 3 mm wide. Furthermore, there is no plane of symmetry within the generator or within either of the resulting "cylindrical" waves. Therefore one cannot scale down very far with any confidence in the quality of the resulting configurations. The data used are listed in Tables I and II.

III. NUMERICAL STUDIES

The finite difference analogs of the Lagrangian equations of motion of a compressible fluid which were used in the 2DL code are described in Appendix B of Ref. 5; Chapter 4 of that work describes the PBX 9404 equation of state and the Forest Fire constants used.

The calculations were performed using 6400 cells, each 2.0 mm square. The volume viscosity constant⁹ was 3.0. The line initiation was simulated by starting the calculation with a four-cell region of PBX 9404 decomposed and with its CJ pressure.

Figures 9-13 show the calculated density contours that have a 0.02-cm³/g interval at the same times as the radiographs in Figs. 2-6. Also shown are the traces of the late-time radiograph profiles. Figures 14-18 show the pressure contours with a 20-kbar interval.

IV. CONCLUSION

The flow resulting from laterally colliding, diverging cylindrical detonation waves in PBX 9404 has been reproduced numerically by use of the Forest Fire explosive burn model in a two-dimensional finite-difference Lagrangian hydrodynamic code. The calculations also reproduce the observed complicated nature of the Mach stem.

These results suggest that detonation waves resulting from initiation by multiple detonators can be modeled by three-dimensional hydrodynamic codes that use the Forest Fire model to describe the heterogeneous detonation wave propagation.

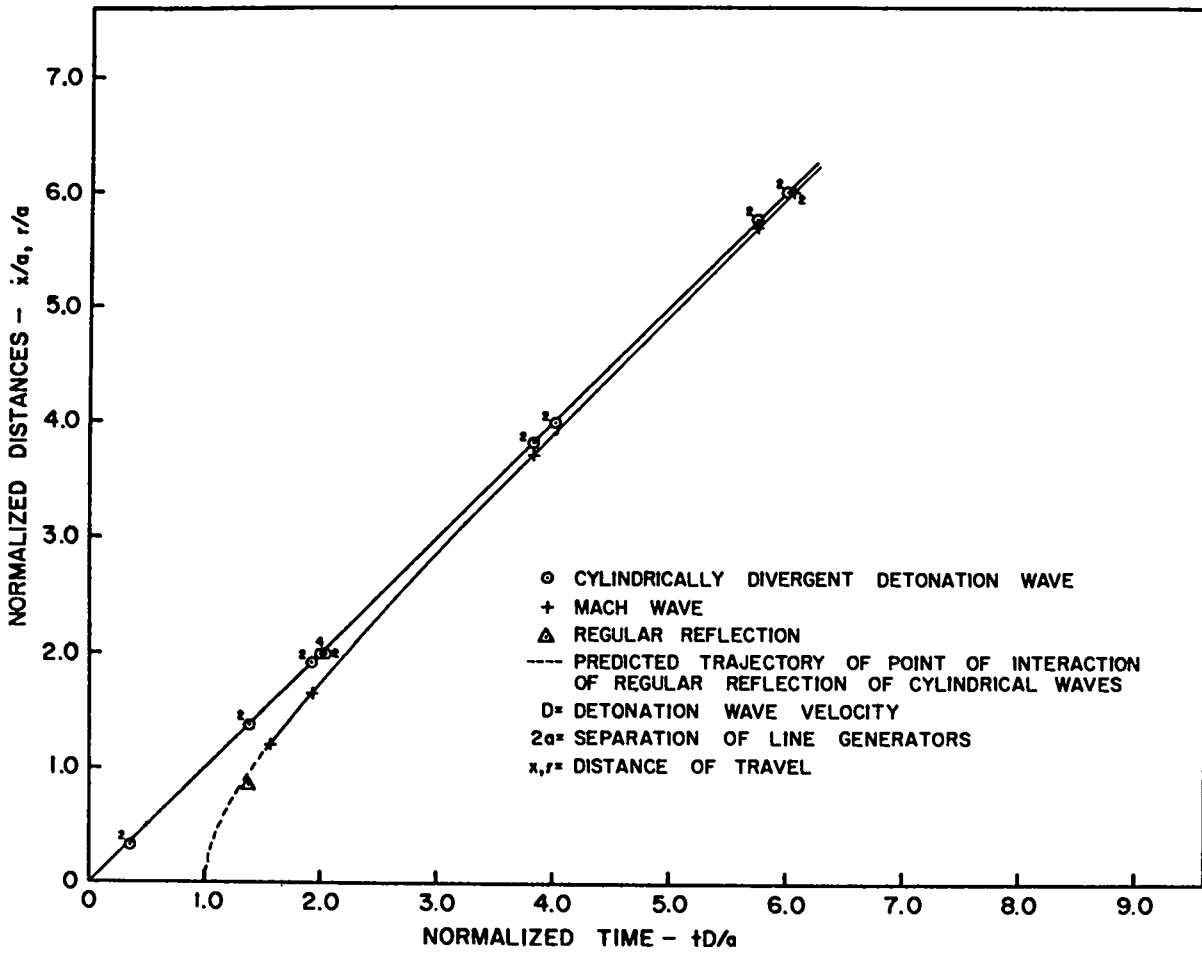


Fig. 7.
Progress of detonation and Mach waves.

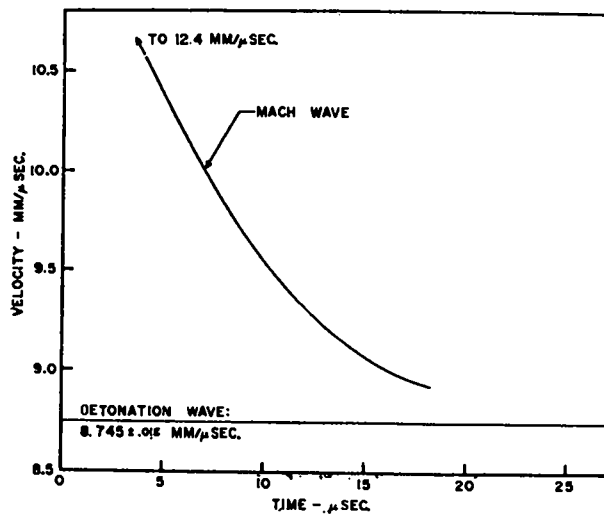


Fig. 8.
Detonation wave and Mach wave velocities.

TABLE I

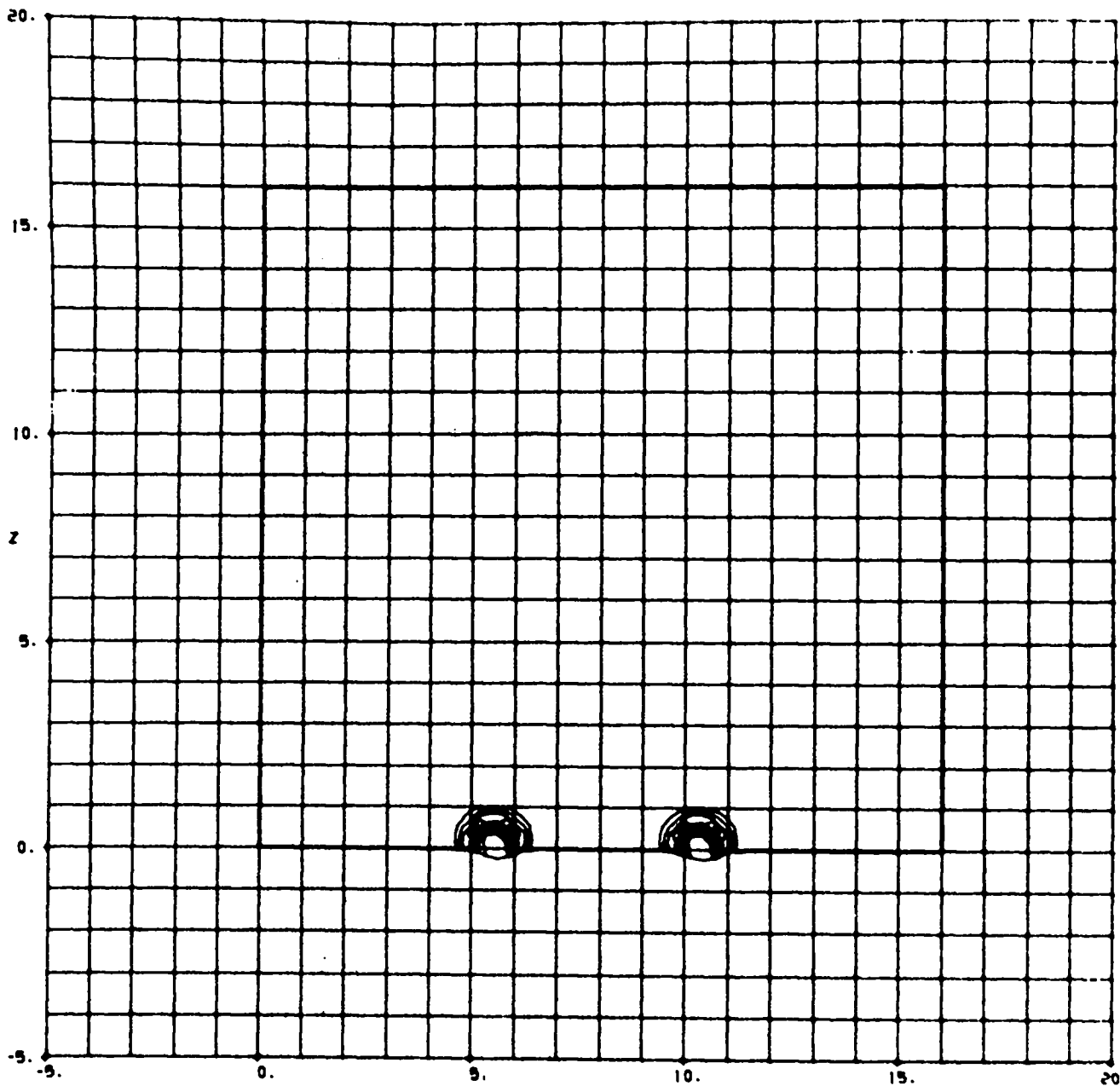
CYLINDRICAL DETONATION
WAVE r AND t DATA

<u>Shot No.</u>	<u>r (mm)</u>	<u>t (μs)</u>	<u>Technique</u>
	0	0	
NW-1130	8.3	1.06	Radiography
NW-1130	8.5	1.06	Radiography
NW-1143	35.0	4.03	Radiography
NW-1143	35.0	4.03	Radiography
NW-1019	49.0	5.61	Radiography
NW-1019	49.0	5.61	Radiography
NW-1130	50.8	5.94	Pin
NW-1130	50.8	5.97	Pin
NW-1143	50.8	5.86	Pin
NW-1143	50.8	5.85	Pin
NW-1019	50.8	5.86	Pin
NW-1019	50.8	5.86	Pin
NW-1037	97.2	11.16	Radiography
NW-1037	97.2	11.16	Radiography
NW-1037	101.6	11.71	Pin
NW-1037	110.6	11.75	Pin
NW-1038	146.2	16.75	Radiography
NW-1038	146.2	16.75	Radiography
NW-1038	152.4	17.49	Pin
NW-1038	152.4	17.49	Pin

TABLE II

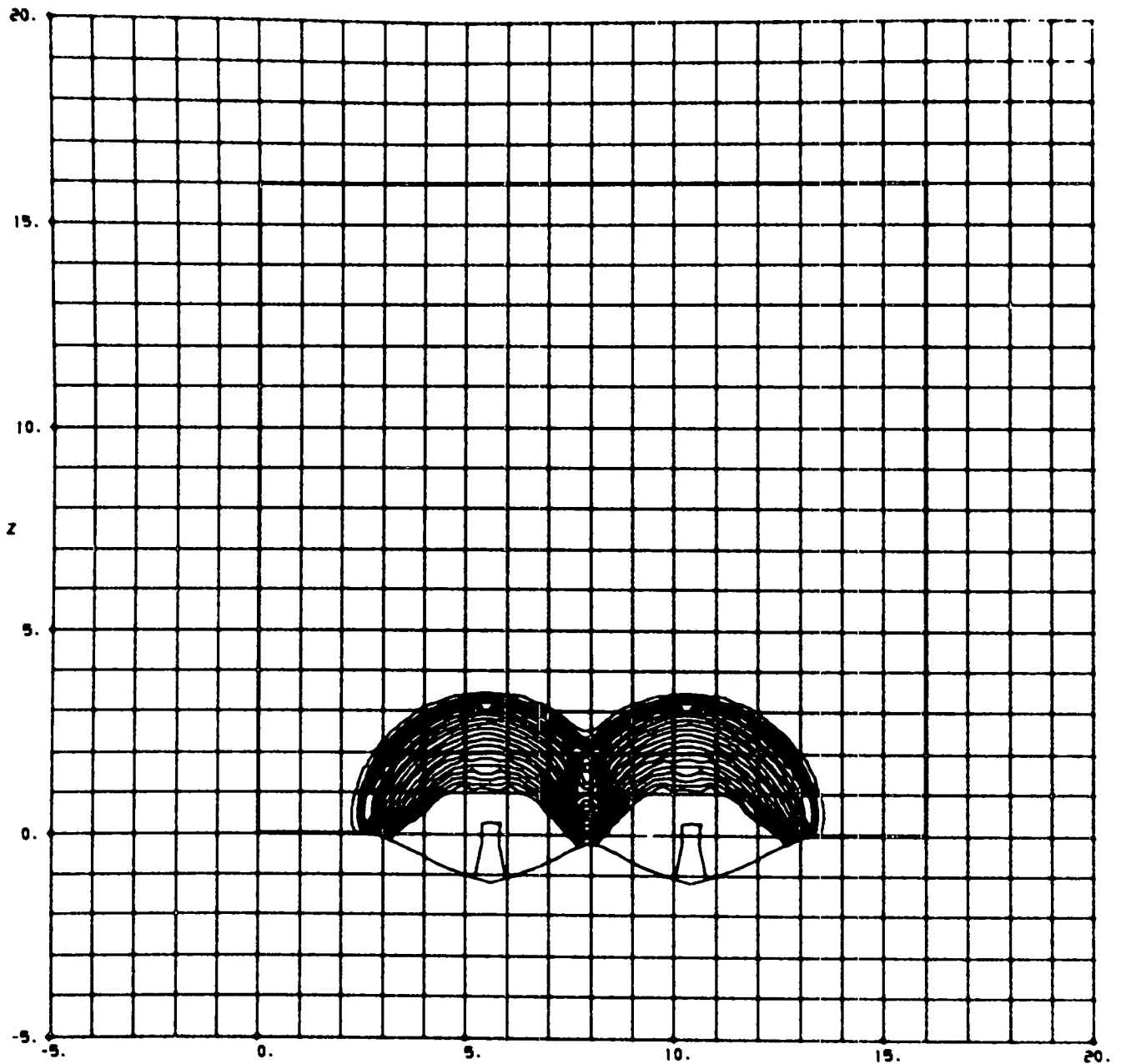
MACH WAVE y AND t DATA

<u>y (mm)</u>	<u>t (μs)</u>
30.5	4.55
42.0	5.61
94.3	11.16
144.7	16.75
152.4	17.66



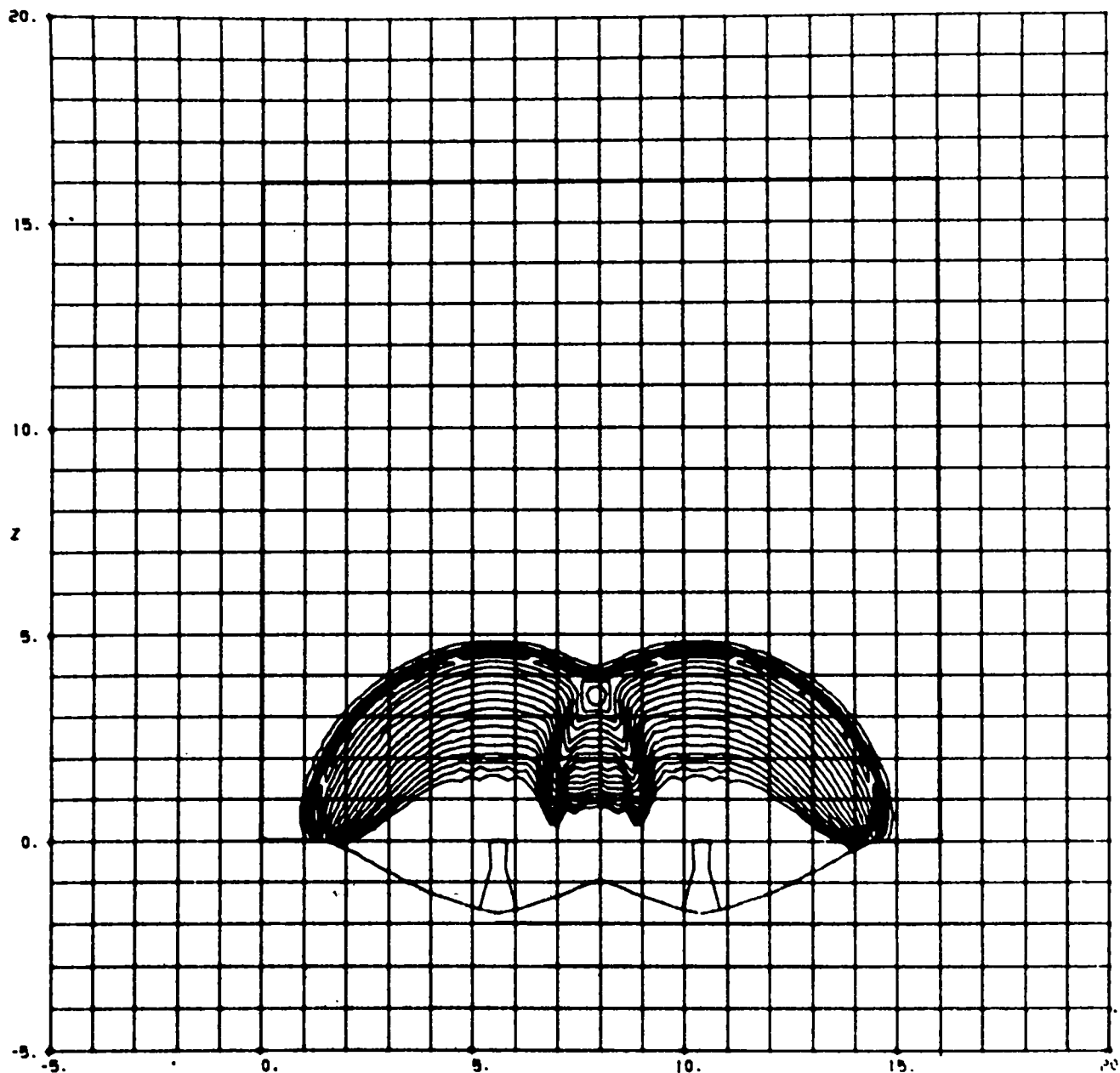
TWO LINE LENSES INITIATING 9404
 VOLUME MIN = 2.5000E-01 MAX = 7.0000E-01 INTV = 2.0000E-02 TIME = 1.0000E+00

Fig. 9
 The calculated isopycnic contours at 1.0 μ s. The contour interval is 0.02 cm^3/g .



TWO LINE LENSES INITIATING 9404
 VOLUME MIN = 2.5000E-01 MAX = 7.0000E-01 INTV = 2.0000E-02 TIME = 4.0000E+00

Fig. 10.
 The calculated isopycnic contours at 4.0 μ s. The contour interval is 0.02 cm^3/g .



TWO LINE LENSES INITIATING 9404
 VOLUME MIN = 2.5000E-01 MAX = 7.0000E-01 INTV = 2.0000E-02 TIME = 5.6000E+00

Fig. 11.

The calculated isopycnic contours at 5.6 μ s. The contour interval is 0.02 cm^3/g .

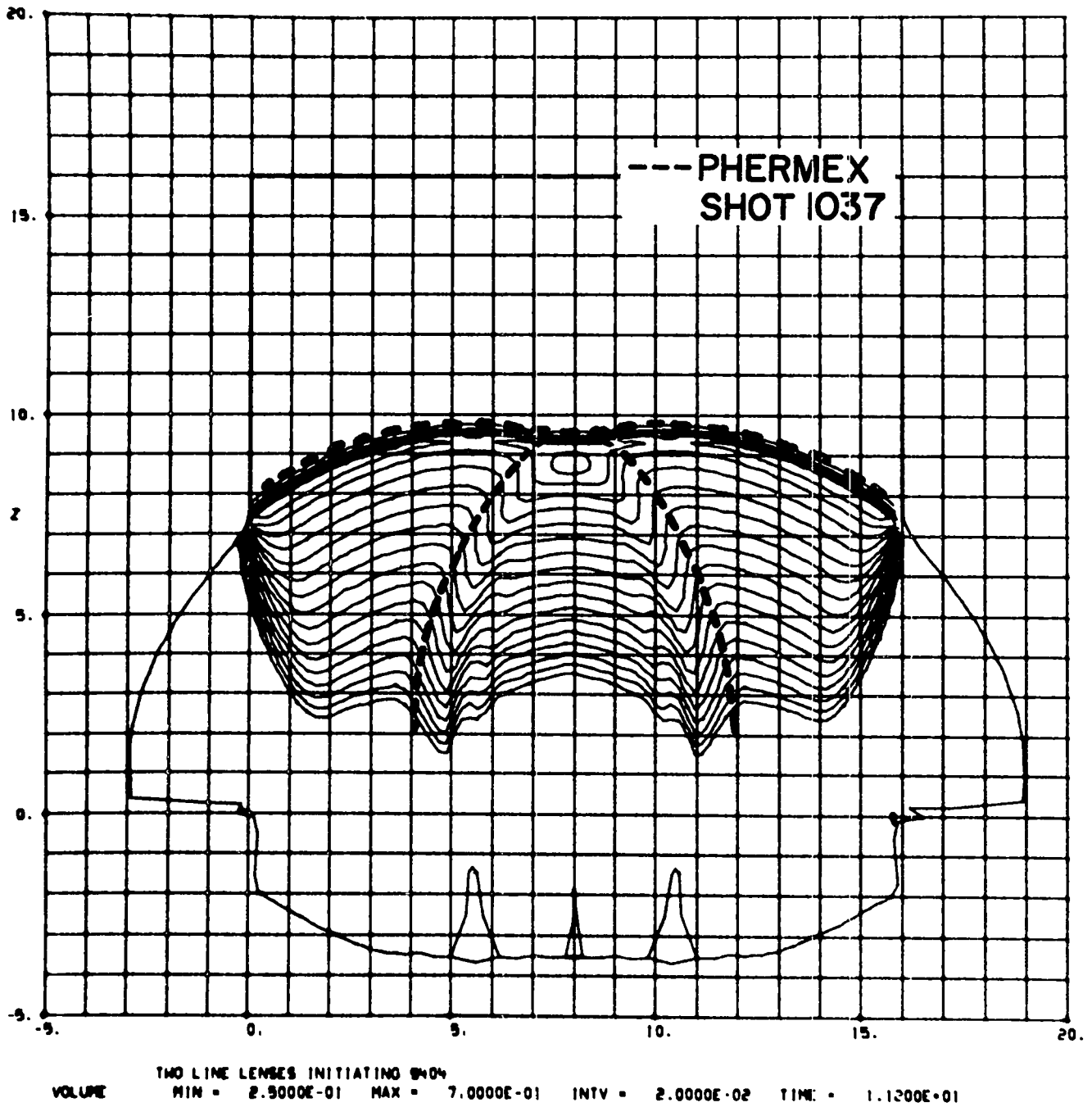


Fig. 12.
The calculated isopycnic contours at 11.2 μ s. The contour interval is 0.02 cm^3/g . The shock-wave profiles from Shot 1037 (Fig. 5) are shown.

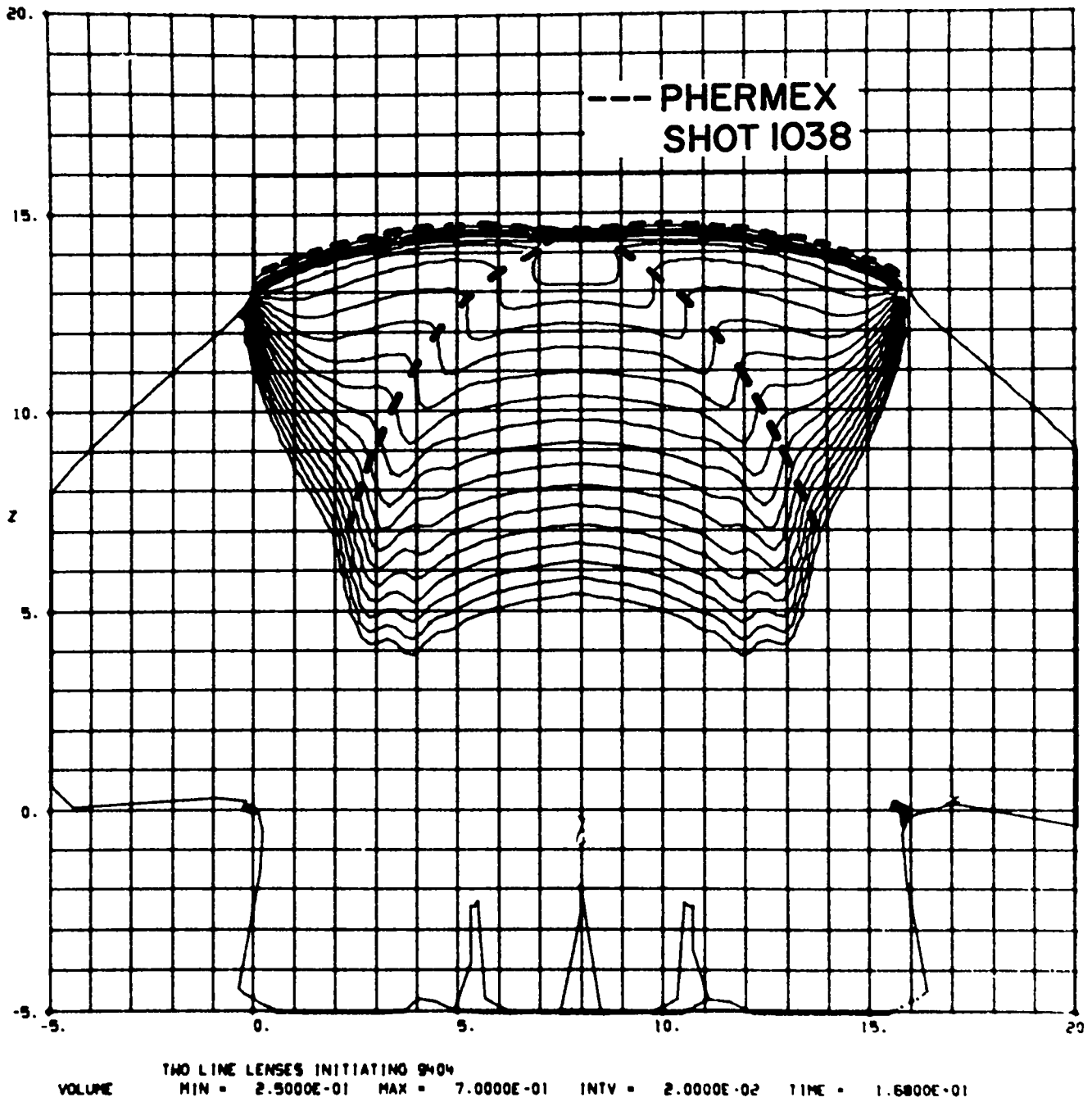
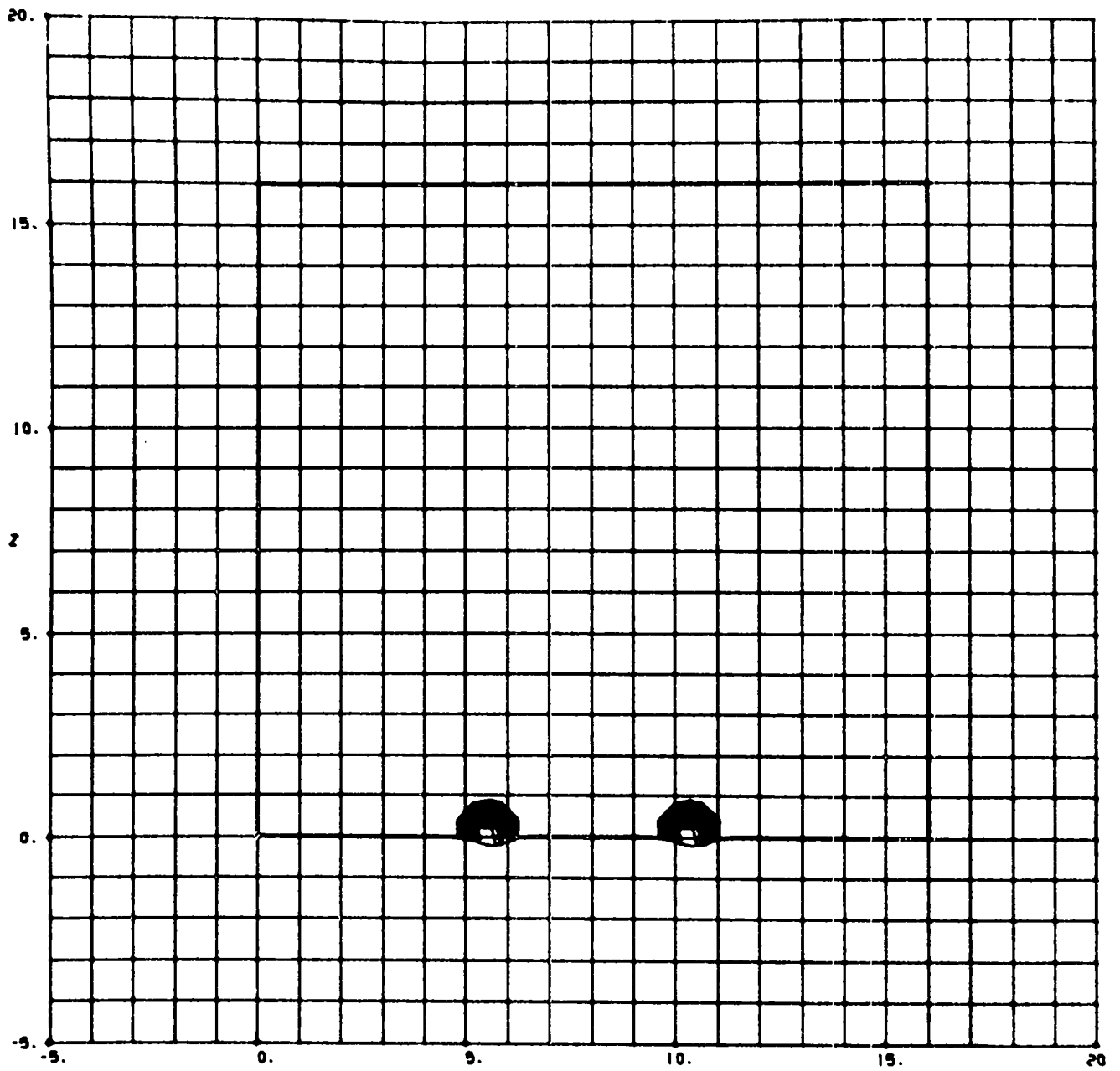
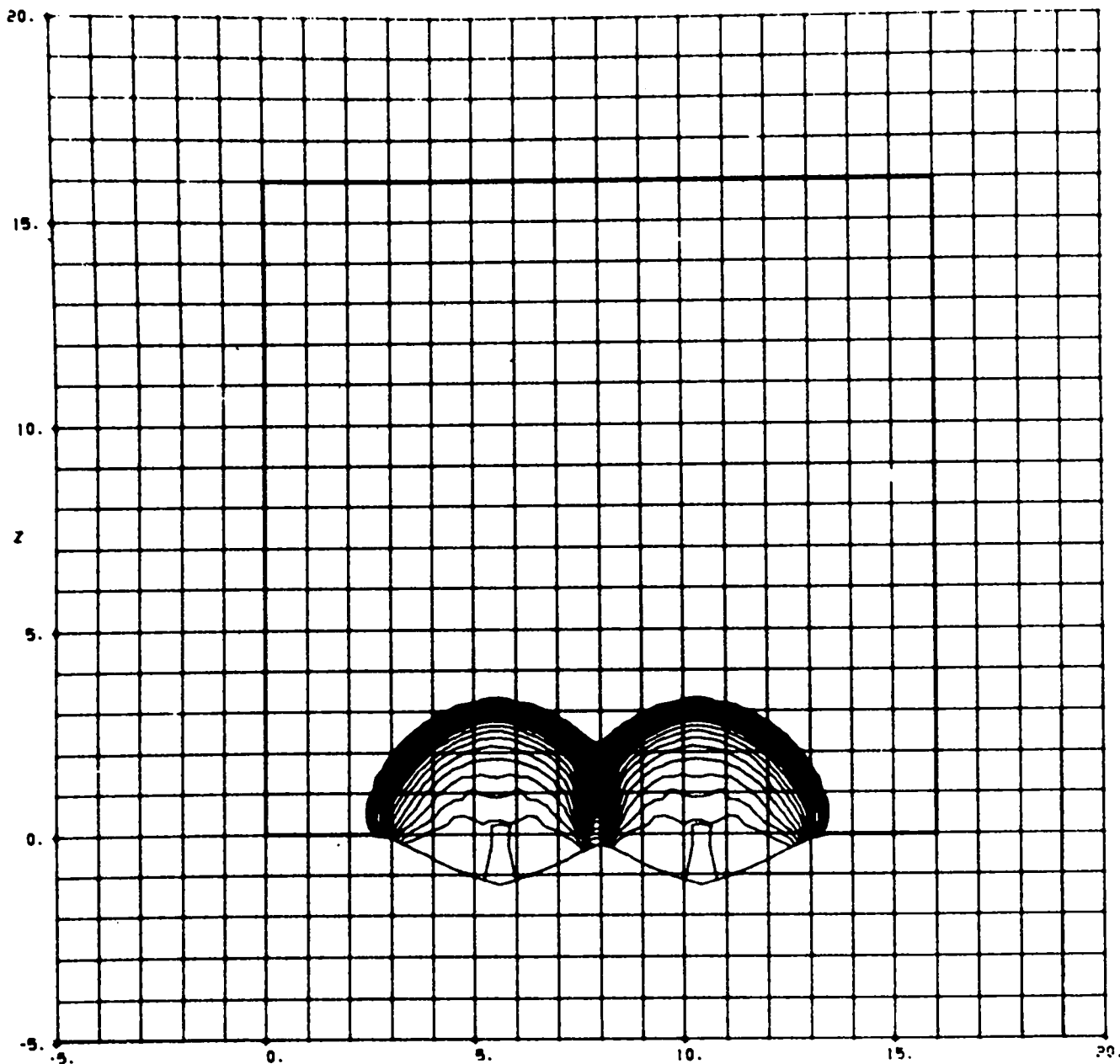


Fig. 13.
The calculated isopycnic contours at 16.8 μ s. The contour interval is 0.02 cm^3/g . The shock wave profiles from Shot 1038 (Fig. 6) are shown.



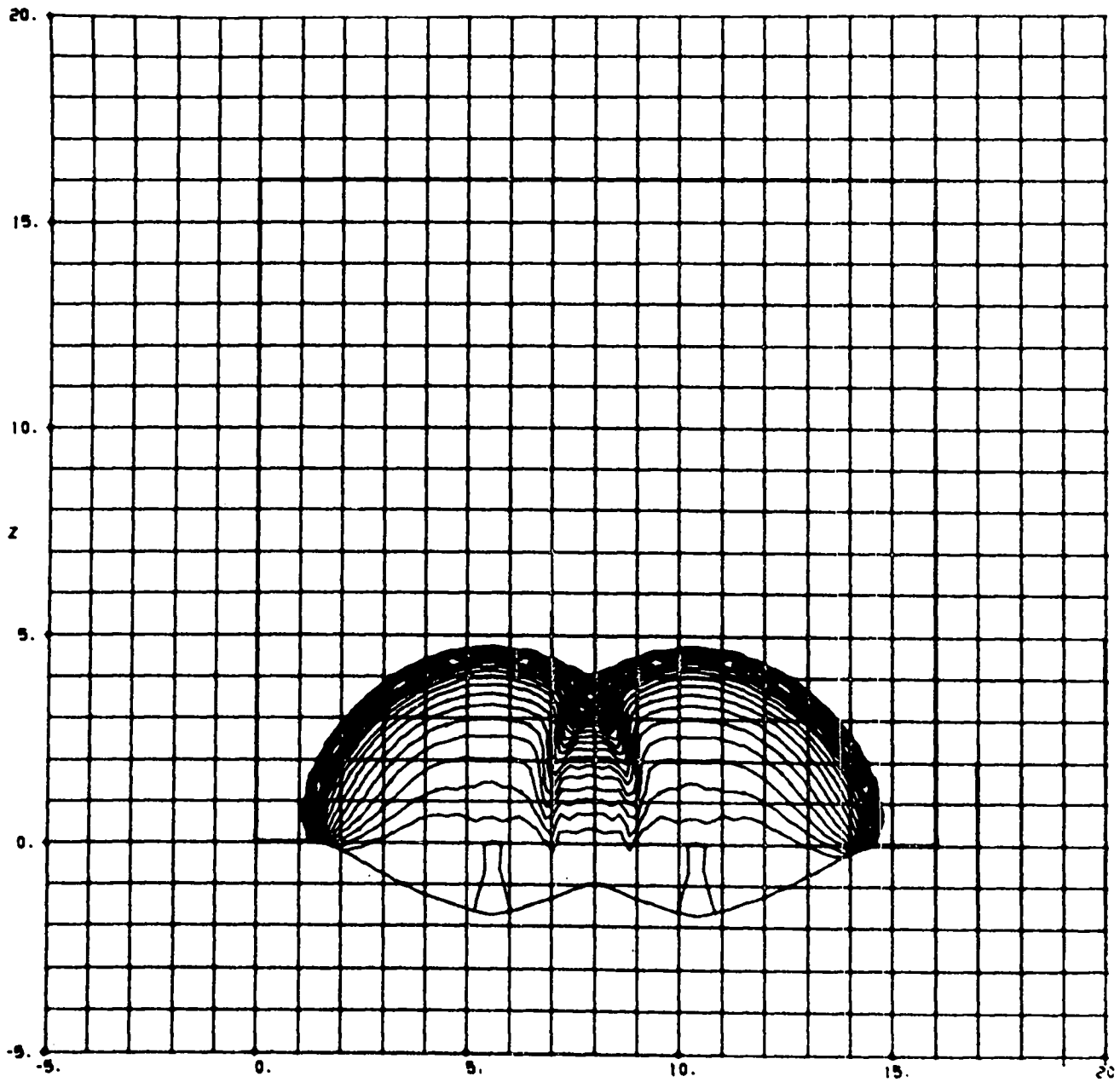
TWO LINE LENSES INITIATING 9404
 PRESSURE MIN = 4.0000E-02 MAX = 1.0000E+00 INTV = 2.0000E-02 TIME = 1.0000E+00

Fig. 14.
 The calculated isobar contours at 1.0 μ s. The contour interval is 20 kbar.



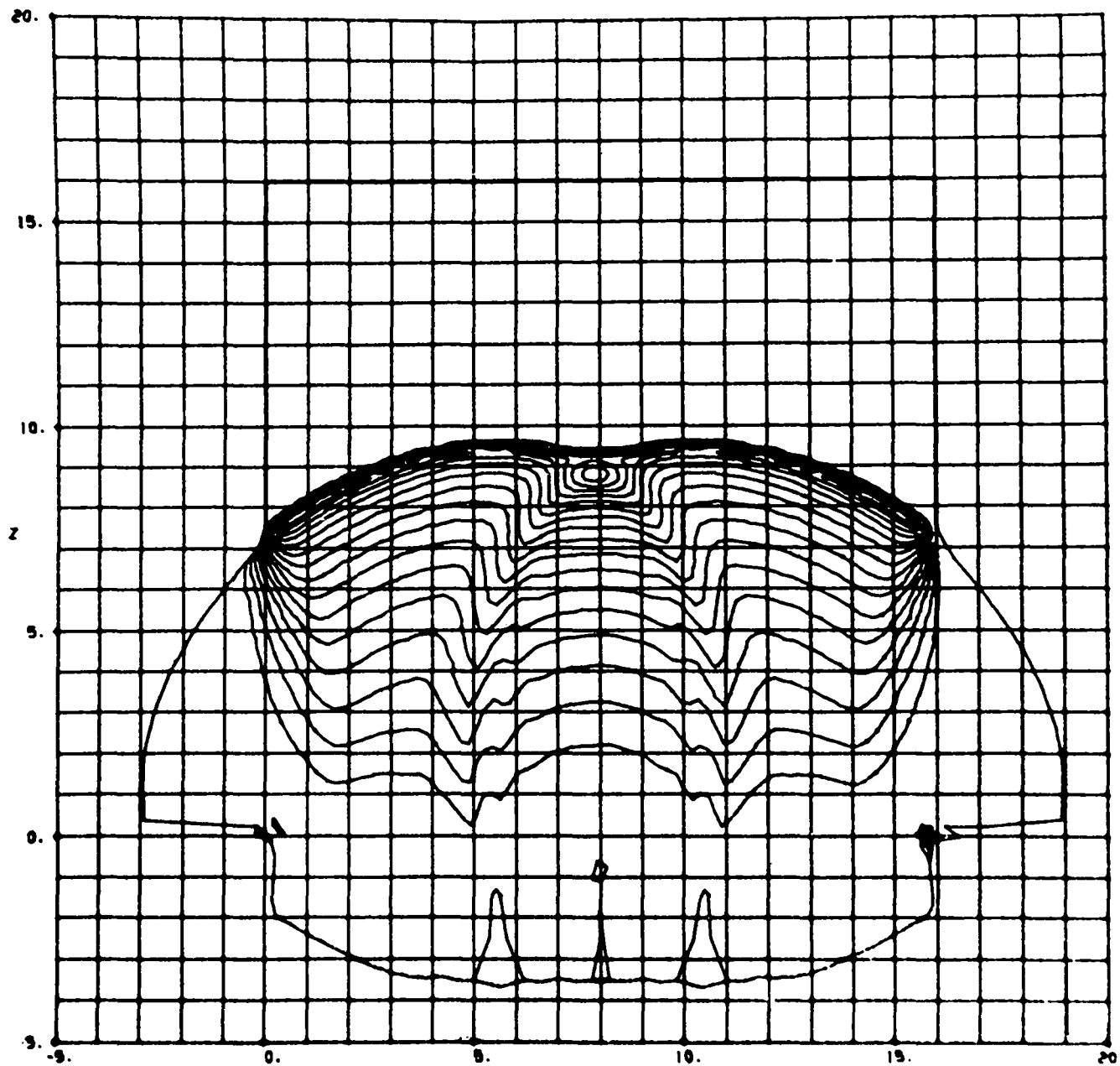
TWO LINE LENSES INITIATING 9+04
 PRESSURE MIN = 4.0000E-02 MAX = 1.0000E+00 INTV = 2.0000E-02 TIME = 4.0000E+00

Fig. 15.
The calculated isobar contours at 4.0 μ s. The contour interval is 20 kbar.



TWO LINE LENSES INITIATING 9404
 PRESSURE MIN = 4.0000E-02 MAX = 1.0000E+00 INTV = 2.0000E-02 TIME = 5.6000E+00

Fig. 16.
 The calculated isobar contours at 5.6 μ s. The contour interval is 20 kbar.



TWO LINE LENSES INITIATING SHOCK
 PRESSURE MIN = 4.0000E-02 MAX = 1.0000E+00 INTV = 2.0000E-02 TIME = 1.1200E+01

Fig. 17.
 The calculated isobar contours at 11.2 μ s. The contour interval is 20 kbar.

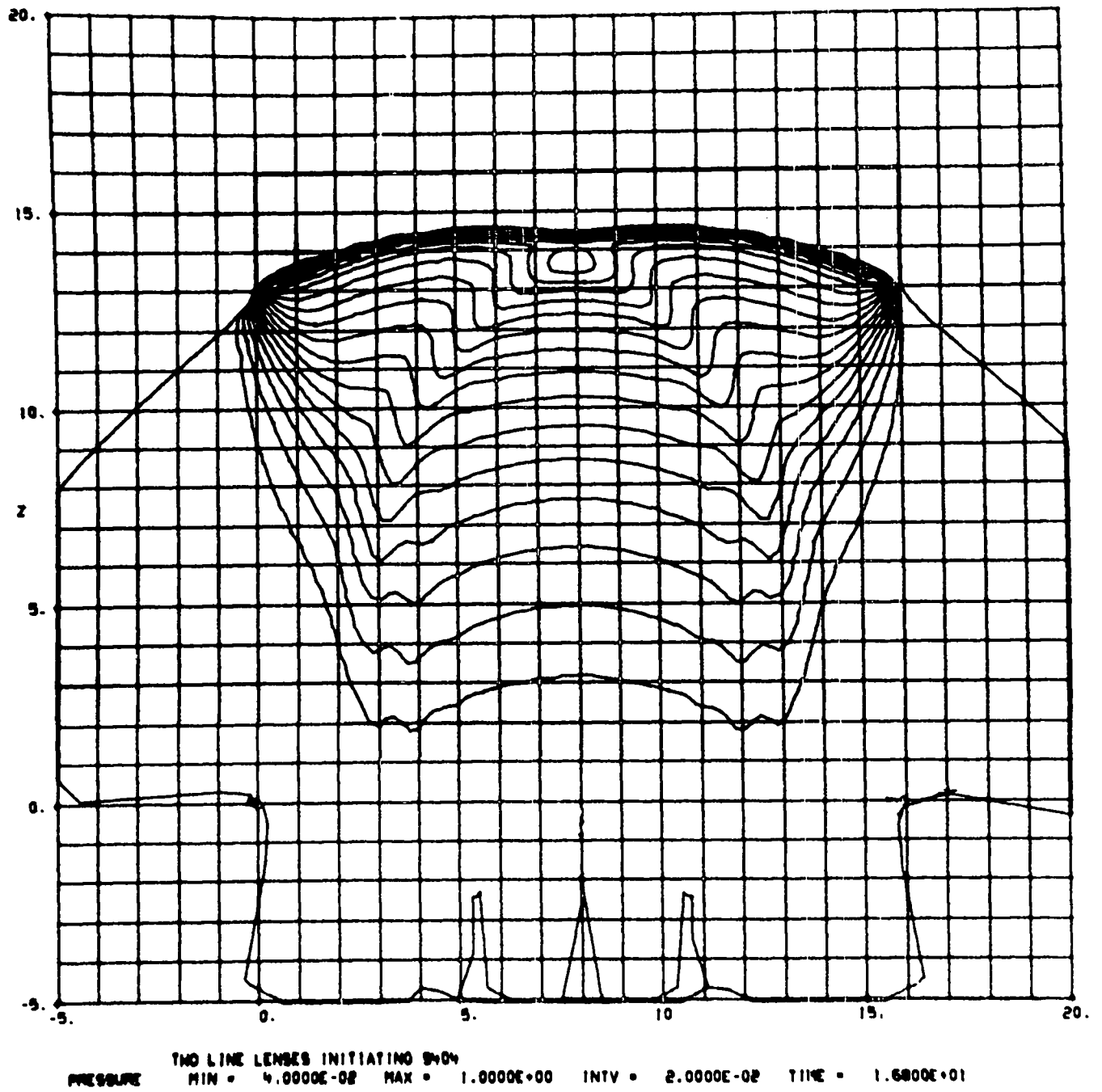


Fig. 18.
 The calculated isobar contours at 16.8 μ s. The contour interval is 20 kbar.

REFERENCES

1. L. V. Al'Tshuler, S. B. Korner, A. A. Bakanova, A. P. Petrunin, A. I. Funtikov, and A. A. Gubkin, *J. Expt. Theoret. Phys. (U.S.S.R.)* 41, 1382 (1961).
2. Charles L. Mader, "Numerical Studies of Regular and Mach Reflection of Shocks in Aluminum," Los Alamos Scientific Laboratory Report LA-3578 (1967).
3. S. D. Gardner and Jerry Wackerle, "Interactions of Detonation Waves in Condensed Explosives," The Fourth Symposium on Detonation, Office of Naval Research Symposium Report ACR-126, 154 (1965).
4. B. D. Lamborn and P. W. Wright, "Mach Interaction of Two Plane Detonation Waves" The Fourth Symposium on Detonation, Office of Naval Research Symposium Report ACR-126, 142 (1965).
5. Charles L. Mader, *Numerical Modeling of Detonations* (University of California Press, Berkeley, California, 1979).
6. D. Venable, "PHERMEX," *Phys. Today* 17, No. 12, 19 (1964).

Printed in the United States of America. Available from
National Technical Information Service
US Department of Commerce
5285 Port Royal Road
Springfield, VA 22161

Microfiche \$3.00

001-025	4.00	126-150	7.25	251-275	10.75	376-400	13.00	501-525	15.25
026-050	4.50	151-175	8.00	276-300	11.00	401-425	13.25	526-550	15.50
051-075	5.25	176-200	9.00	301-325	11.75	426-450	14.00	551-575	16.25
076-100	6.00	201-225	9.25	326-350	12.00	451-475	14.50	576-600	16.50
101-125	6.50	226-250	9.50	351-375	12.50	476-500	15.00	601-up	

Note: Add \$2.50 for each additional 100-page increment from 601 pages up.